

CANGAROO-III SEARCH FOR GAMMA RAYS FROM CENTAURUS A AND THE ω CENTAURI REGION

S. KABUKI¹ R. ENOMOTO² G. V. BICKNELL³ R. W. CLAY⁴ P. G. EDWARDS⁵ S. GUNJI⁶ S. HARA⁷ T. HATTORI⁸ S. HAYASHI⁹
Y. HIGASHI¹ R. INOUE⁸ C. ITOH⁷ F. KAJINO⁹ H. KATAGIRI¹⁰ A. KAWACHI⁸ S. KAWASAKI² T. KIFUNE² R. KIUCHI²
K. KONNO⁶ H. KUBO¹ J. KUSHIDA⁸ Y. MATSUBARA¹¹ T. MIZUKAMI¹ R. MIZUNIWA⁸ M. MORI² H. MURAIISHI¹² T. NAITO¹³
T. NAKAMORI¹ D. NISHIDA¹ K. NISHIJIMA⁸ M. OHISHI² Y. SAKAMOTO⁸ V. STAMATESCU⁴ S. SUZUKI¹⁴ T. SUZUKI¹⁴
D. L. SWABY⁴ T. TANIMORI¹ G. THORNTON⁴ F. TOKANAI⁶ K. TSUCHIYA¹ S. WATANABE¹ Y. YAMADA⁹ M. YAMAZAKI⁹
S. YANAGITA¹⁴ T. YOSHIDA¹⁴ T. YOSHIKOSHI² M. YUASA² Y. YUKAWA²

To appear in *ApJ*.

ABSTRACT

We have observed the giant radio galaxy Centaurus A and the globular cluster ω Centauri in the TeV energy region using the CANGAROO-III stereoscopic system. The system has been in operation since 2004 with an array of four Imaging Atmospheric Cherenkov Telescopes (IACT) with ~ 100 -m spacings. The observations were carried out in March and April 2004. In total, approximately 10 hours data were obtained for each target. No statistically significant gamma-ray signal has been found above 420 GeV over a wide angular region (a one-degree radius from the pointing center) and we derive flux upper limits using all of the field of view. Implications for the total energy of cosmic rays and the density of the cold dark matter are considered.

Subject headings: gamma rays: search — galaxy: individual (Centaurus A) — globular cluster: individual (ω Centauri)

1. INTRODUCTION

Centaurus A (Cen A, NGC 5128, J1325–4301) is one of the best examples of a radio-loud AGN. Viewed at $\sim 60^\circ$ from the jet axis (Graham et al. 1979; Dufour et al. 1979; Jones et al. 1996), it has been classified as a “misaligned” BL Lac type AGN (Morganti et al. 1992). Estimates of the distance to Cen A range from 2 to 8 Mpc. In this paper, we adopt a value of 3.5 Mpc (Hui et al. 1993). Due to its proximity and high luminosity, Cen A has long been considered a good TeV gamma-ray candidate. A detection of high energy gamma-rays from Cen A was reported in the 1970s, however many subsequent attempts have not been successful.

First, the Stellar Interferometer, located near Narrabri,

¹ Department of Physics, Kyoto University, Sakyo-ku, Kyoto 606-8502, Japan

² Institute for Cosmic Ray Research, University of Tokyo, Kashiwa, Chiba 277-8582, Japan

³ Research School of Astronomy and Astrophysics, Australian National University, ACT 2611, Australia

⁴ School of Chemistry and Physics, University of Adelaide, SA 5005, Australia

⁵ Paul Wild Observatory, CSIRO Australia Telescope National Facility, Narrabri, NSW 2390, Australia

⁶ Department of Physics, Yamagata University, Yamagata, Yamagata 990-8560, Japan

⁷ Ibaraki Prefectural University of Health Sciences, Ami, Ibaraki 300-0394, Japan

⁸ Department of Physics, Tokai University, Hiratsuka, Kanagawa 259-1292, Japan

⁹ Department of Physics, Konan University, Kobe, Hyogo 658-8501, Japan

¹⁰ Department of Physical Science, Hiroshima University, Higashi-Hiroshima, Hiroshima 739-8526, Japan

¹¹ Solar-Terrestrial Environment Laboratory, Nagoya University, Nagoya, Aichi 464-8602, Japan

¹² School of Allied Health Sciences, Kitasato University, Sagami-hara, Kanagawa 228-8555, Japan

¹³ Faculty of Management Information, Yamanashi Gakuin University, Kofu, Yamanashi 400-8575, Japan

¹⁴ Faculty of Science, Ibaraki University, Mito, Ibaraki 310-8512, Japan

reported a positive detection with a flux of $I(> 0.3 \text{ TeV}) \sim (4.4 \pm 1) \times 10^{-11} \text{ photon cm}^{-2} \text{ sec}^{-1}$ (Grindlay et al. 1975).

At higher energies, the Buckland Park array and the JANZOS Observatory also reported the detection of gamma-rays. The Buckland Park flux, measured between 1984 and 1989, was $I(> 100 \text{ TeV}) \sim (7.4 \pm 2.6) \times 10^{-12} \text{ photon cm}^{-2} \text{ sec}^{-1}$ (Clay et al. 1994) and the JANZOS flux, during the period Apr–Jun 1990, was $I(> 110 \text{ TeV}) \sim (5.5 \pm 1.5) \times 10^{-12} \text{ photon cm}^{-2} \text{ sec}^{-1}$ (Allen et al. 1993). Given the significant attenuation expected in the gamma-ray flux during interactions with the cosmic microwave background at these energies, these measured fluxes imply much greater intrinsic fluxes (Protheroe 1986).

However, CANGAROO-I (Rowell et al. 1999), JANZOS (long-term) (Allen et al. 1993, b), and Durham (Caramiñana et al. 1990) observed the Cen A nuclear region and set upper limits on the emission in the VHE range. Recently, the H.E.S.S. group observed Cen A for 4.2 hours in 2004 (Aharonian et al. 2005c). Their upper limit was $5.68 \times 10^{-12} \text{ photon cm}^{-2} \text{ sec}^{-1}$ (1.9% of the Crab flux) at 190 GeV. They only investigated the region close to the center of Cen A, i.e., the inner jet region. Cen A has a large structure revealed by the radio observations, with inner lobes extending over ~ 10 arcmin, a middle lobe extending over ~ 1 degree, and outer lobes extending over more than 5 degrees (Burns, Feigelson, & Schreier 1983). The fluxes obtained in those observations are plotted in Fig. 1. The details of the observations are listed in Table 1.

Cen A has displayed pronounced variability at X-ray energies over the last 35 years, with the Grindlay et al. detection coinciding with the peak of the X-ray flux over this period (see, e.g., Turner et al. 1997). Data from the ROSAT All Sky Monitor (ASM 2007), indicate that in recent years, including the period of the H.E.S.S. observations, Cen A has been near its historical minimum X-ray state (MJD from 53111 to 53113).

TABLE 1
DETAILS OF PAST OBSERVATIONS.

mark ^a	reference	epoch	threshold	significance	method
G	Grindlay et al. (1975)	1972–1974	300 GeV	4.5 σ	Cherenkov ^{b c}
J3	Allen et al (1993)	Apr–Jun 1990	110 TeV	2% ^d	Shower Array
J2	Allen et al (1993)	1987–1992	110 TeV	95% CL. UL.	Shower Array
B	Clay et al. (1994)	1984–1989	100 TeV	99.4% CL.	Shower Array
J1	Allen et al (1993b)	1988 & 1989	1 TeV	95% CL. UL.	Cherenkov ^b
D	Carramiñana et al. (1990)	1987 & 1988	300 GeV	3 σ UL.	Cherenkov ^b
CI	Rowell et al. (1999)	Mar–Apr 1995	1.5 TeV	3 σ UL.	IACT
H	Aharonian et al. (2005c)	Apr 2004	190 GeV	99% CL. UL.	stereoscopic IACT

^aMark in Fig. 1.

^bNo imaging Cherenkov telescope.

^cSpectral index consistent with $\gamma=-1.7$.

^dChance probability.

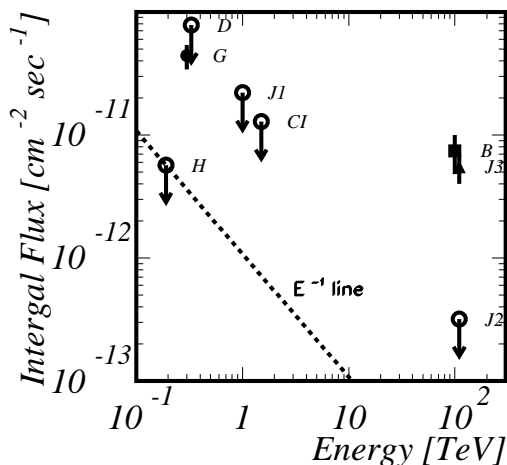


FIG. 1.— Summary of the past observations. The filled marks are the positive detection and the open upper limits. The details of these observations were listed in Table 1. The dashed line is a spectrum proportional to E^{-1} with H.E.S.S.’s upper-limit level flux.

CANGAROO-III has data outside of this minimum period (MJD from 530080 to 530107). We also report the results over a wide region. Part of the southern outer lobe of Cen A was located within the field of observations made of ω Centauri (ω Cen). We, therefore, include the results of the latter observation in this report. Located at a distance of 4.9 kpc, ω Cen is one of the oldest, heaviest globular clusters in our Galaxy. As globular clusters have been found to contain large numbers of millisecond pulsars, they are interesting objects for high-energy gamma ray observations.

2. CANGAROO-III STEREOSCOPIC SYSTEM

The use of imaging atmospheric Cherenkov telescopes (IACTs) was established with the statistically unassailable detection of the Crab nebula at TeV energies by the Whipple group (Weekes et al. 1989). This technique enables TeV gamma-rays to be selected from the huge background of cosmic rays with the use of the “image moments” of the shower images (Hillas 1985). Stereoscopic

observations, which allow the signal-to-noise ratio to be significantly improved, were pioneered by the HEGRA group (Aharonian et al. 1999). The H.E.S.S. group has recently reported the detection of faint gamma-ray sources with an angular resolution as fine as a few arcminutes (Aharonian et al. 2005).

CANGAROO-III is one of two major IACTs located in the southern hemisphere. The CANGAROO-III stereoscopic system consists of four imaging atmospheric Cherenkov telescopes located near Woomera, South Australia (31°S, 137°E). Each telescope has a 10 m diameter segmented reflector, consisting of 114 spherical mirrors made of FRP (Kawachi et al. 2001), each of 80 cm diameter, mounted on a parabolic frame with a focal length of 8 m. The total light collecting area is 57.3 m². The first telescope, T1, which was the CANGAROO-II telescope, is not presently in use due to its smaller field of view and higher energy threshold. The second, third, and fourth telescopes (T2, T3, and T4) were used for the observations described here. The camera systems for T2, T3, and T4 are identical and their details are given in Kabuki et al. (2003). The telescopes are located at the east (T1), west (T2), south (T3) and north (T4) corners of a diamond with sides of ~ 100 m (Enomoto et al. 2002b).

3. OBSERVATIONS

The observations were carried out in the period from 2004 March 16 to April 19 using “wobble mode” in which the pointing position of each telescope was shifted in declination between ± 0.5 degree every 20 minutes (Daum et al. 1997) from each target: (RA, dec [J2000]) = (201.365°, -43.019°) for Cen A, (RA, dec [J2000]) = (201.691°, -47.477°) for ω Cen. One of the reason why we took “wobble” observation is to enlarge the effective FOV, the other is to average the responses of individual pixels. We, therefore, took LONG OFF source run of “wobble” mode for background subtractions in the later analysis.

Data with GPS time stamps were recorded for T2, T3 and T4 individually when more than four photomultiplier (PMT) signals exceeded 7.6 photoelectrons (p.e.). In the offline analysis stage we combine all these data when the three telescope’s GPS times coincide. The typical trigger rate was 11 Hz for three-fold coincidences. Each night was divided into two or three periods, i.e., ON-OFF,

OFF-ON-OFF, or OFF-ON observations. ON-source observations were timed to contain the meridian passage of the target. On average the OFF source regions were located with an offset in RA of $+30^\circ$ or -30° from the target. The OFF-source observations were also made in wobble mode. One day was dedicated to ON and OFF source observations of one target, with the following day dedicated to the other target. The images in all three telescopes were required to have clusters of at least five adjacent pixels exceeding a 5 p.e. threshold (three-fold coincidence). The event rate was reduced to ~ 7.5 Hz by this criterion. Looking at the time dependence of these rates, we can remove data taken in cloudy conditions. This procedure is the same as the ‘‘cloud cut’’ used in the CANGAROO-II analysis (Enomoto et al. 2002). The effective observation times for ON and OFF source observations were 639.4 and 586.9 min for Cen A, and 600.8 and 429.4 min for ω Cen. The mean zenith angles were 17.4° and 20.6° , respectively.

The light collecting efficiencies, including the reflectivity of the segmented mirrors, the light guides, and the quantum efficiencies of photomultiplier tubes were monitored by a muon-ring analysis (Enomoto et al. 2006) with the individual trigger data in the same periods. The light yield per unit arc-length is approximately proportional to the light collecting efficiencies. The average ratios of these at the observation period with respect to the mirror production times (indicating the amount of deterioration) were estimated to be 70, 70, and 80% for T2, T3, and T4, respectively. The measurement errors are considered to be at less than the 5% level. Deterioration is mostly due to dirt and dust settling on the mirrors.

4. ANALYSIS

Most of the analysis procedures used are identical with those described in Enomoto et al. (2006b). As a full instrumental description was given in Enomoto et al. (2006), we omit a detailed discussion here. There are some improvements in the analysis procedure from that in the previous paper and so we concentrate on those points here.

At first, the image moments (Hillas 1985) were calculated for the three telescopes’ images. The gamma-ray’s incident directions were determined by minimizing the sum of squared widths (χ_0^2 : weighted by the photon yield) of the three images seen from the assumed position (fitting parameter) with a constraint on the distances from the intersection point to each image center (D_{IP}). The D_{IP} can be estimated from the ratio $Length/Width$. The prediction curve (f) and its error (σ) were estimated using Monte-Carlo simulations. The constraint is;

$$\chi_c^2 = \frac{[D_{IP} - f(Length/Width)]^2}{\sigma^2}.$$

In order to balance dimensions between χ_0^2 and χ_c^2 , we need to multiply $n \cdot \langle Width^2 \rangle$ by χ_c^2 , where n has the units of number of photo-electrons (p.e.) and is optimized by Monte-Carlo simulations ($n=10$ p.e. for this analysis). Finally the minimizing variable is;

$$\chi^2 = \chi_0^2 + n \cdot \langle Width^2 \rangle \cdot \chi_c^2.$$

For large images, the former term dominates and for small images (for example, events at large zenith angles),

the latter dominates. With this fit, we can improve uniformity of θ^2 resolution especially with respect to zenith angle.

In order to derive the gamma-ray likeliness, we used the Fisher Discriminant (hereafter FD) (Fisher 1936; Enomoto et al. 2006). Input parameters were

$$\vec{P} = (W2, W3, W4, L2, L3, L4),$$

where $W2, W3, W4, L2, L3, L4$ are energy corrected $Widths$ and $Lengths$ for the T2, T3, and T4. FD has a small dependence on the zenith angle, i.e., as the zenith becomes larger, images become smaller (FD larger). We corrected for this using Monte-Carlo simulations.

We rejected events with any hits in the outermost layer of the cameras (‘‘edge cut’’). These rejected events cause finite deformations especially in the $Length$ distribution which results in deformations of the FD . In this analysis, we allowed less energetic hit pixels on the ‘‘edge’’ layer if their pulse heights were less than that of highest 15 pixels. This cut was improved in order to increase acceptance.

Since we have FD distributions for OFF-source data and the Monte-Carlo gamma-ray events, we can assume these are background and signal events respectively. Note that in the gamma-ray simulations we used a spectrum proportional to E^γ where $\gamma=-2.1$. We can therefore fit the FD distribution of ON with the above emulated signal and real background functions, to derive the number of signal events passing the selection criteria. With this fit, we can determine the gamma-ray excess without any positional subtractions. This is a one-parameter fitting with the constraint that sum of signal and background events corresponds to the total number of events. These coefficients can be derived exactly analytically.

5. RESULTS

The morphology (significance map) is shown in Fig. 2.

The FOV was binned to 0.2 degree \times 0.2 degree squares. The FD distribution inside each bin was made. The signal function (for gamma rays) was made using the Monte-Carlo simulation. The background (for protons) function was made collecting OFF events inside 0.6×0.6 degree² centered around the corresponding signal bin. The one-parameter χ^2 fit was carried out and the excess counts were obtained inside a one-degree circle (the dot-dashed circle) centered at the average pointing position. The pointing centers are shown by the crosses. At one degree radius, the acceptance decreases by 30%. There is, therefore, not any statistically significant excess anywhere. The positive and negative fluctuations roughly agree in the Cen A field of view. In that of ω Cen a positive offset was observed ($\sim 0.4 \sigma$), however, it is not statistically significant. The peak located at north of ω -Cen field and its significance is 1.5σ . The point spread function (PSF) is shown by the dashed circle at left-lower place. The solid contours are obtained via Skyview (2007) and are the GB6 radio data (4850 MHz) showing the inner lobes and middle lobe, and the dotted contours are 408 MHz radio data, roughly showing the outer lobes of Cen A from Fig. 11 of Burns, Feigelson, & Schreier (1983).

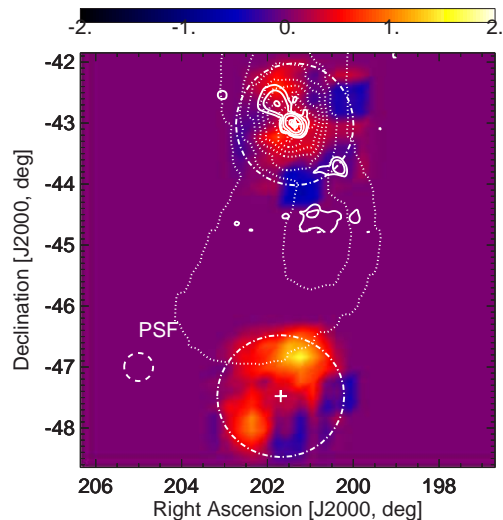


FIG. 2.— Significance map. The angular bins are 0.2×0.2 degree² squares. This was obtained by the fitting procedure described in the text. For the background function of the fit, the OFF region of a 0.6×0.6 deg² square centered on (but not including) the corresponding bin was used. The smoothing was carried out averaging the neighboring bins. The crosses are the pointing centers. Events within one degree radius circles are plotted (the dot-dashed circle). The point spread function (PSF) is shown by the dashed circle. The solid contours are 4850 MHz radio data of the inner lobes and middle lobe and the dotted contours are 408 MHz observations of the outer lobes.

In order to derive a UL for a point source, we choose $\theta^2=0.06$ degree² from the center of Cen A for the cut position. The 2σ UL was obtained to be 39.8 events. The energy threshold for this analysis was obtained to be 424 GeV by the Monte-Carlo simulation. For ω -Cen, a 2σ UL of 32.3 events was obtained.

In order to derive flux ULs for the jet and lobes of Cen A, and ω Cen, we defined the search regions as shown in Fig. 3. Region 1 contains the jet and inner lobes of Cen A, region 3 contains the middle lobe, and regions 4 and 5 contain portions of the outer lobes, while region 2 contains ω Cen. There is no high-energy astronomical counterpart in region 6 (although low level radio emission from the southern outer lobe of Cen A may extend into this region). The flux upper limits for various regions were obtained from the FD distributions of the ON-source runs for corresponding areas. The OFF-source runs were used for the background FD functions and the Monte-Carlo simulations for gamma rays for the signal. We do not observe any statistically significant excesses in any regions.

Thus we can obtain flux ULs for region 1. Those of Cen A center region are summarized in Table 2. ULs are

TABLE 2
FLUX UPPER LIMITS ABOVE VARIOUS ENERGY THRESHOLDS FOR THE CEN A JET

Excess Upper Limit	Energy Threshold	Flux Upper Limit
Events	GeV	cm ² s ⁻¹
39.8	424	0.491×10^{-11}
12.6	2074	0.903×10^{-12}
5.0	6202	0.485×10^{-12}

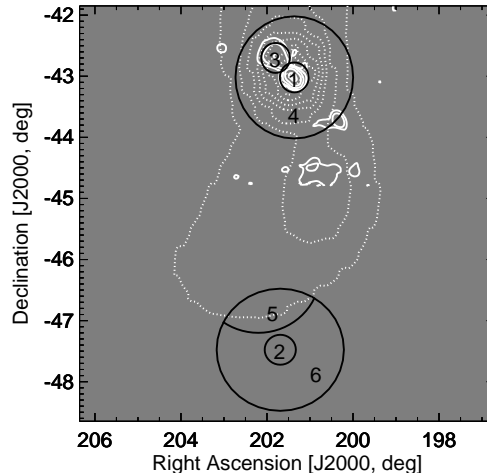


FIG. 3.— Definition of search regions. Region 1 contains the jet and inner lobes of Cen A and region 2 is ω Cen. These sizes are identical to the PSF. Region 3 is the middle lobe of Cen A, centered at (RA, dec [J2000]) = (201°.95, -42°.85). The size is identical to the PSF. Region 4 is within a one-degree circle from the center of Cen A not including regions 1 and 3: which contains portions of the outer lobes of Cen A close to the nucleus. Region 5 is the overlap of two one-degree circles centered at (RA, dec)=(205°, -47°) and ω Cen: the southern extremity of the outer lobe of Cen A (Burns, Feigelson, & Schreier 1983). Region 6 is within one-degree circle from the center of ω Cen not including regions 2 and 5.

presented for three different energy thresholds.

Exactly the same procedure was carried out for the ω Cen region. Again there is no statistically significant excesses. The flux ULs for region 2 are summarized in Table 3. The flux ULs for the regions 3, 4, 5, and 6 are

TABLE 3
FLUX UPPER LIMITS ABOVE VARIOUS ENERGY THRESHOLDS FOR ω CEN

Excess Upper Limit	Energy Threshold	Flux Upper Limit
Events	GeV	cm ² s ⁻¹
32.3	471	0.355×10^{-11}
7.9	2216	0.519×10^{-12}
7.0	6518	0.602×10^{-12}

summarized in Table 4. Here, the ULs are divided by the

TABLE 4
FLUX UPPER LIMITS FOR THE OTHER REGIONS

Region	Excess Upper Limit	Energy Threshold	Flux Upper Limit
	Events	GeV	cm ² s ⁻¹ Sr ⁻¹
3	37.3	424	0.875×10^{-7}
4	132.6	424	0.193×10^{-7}
5	203.7	471	0.106×10^{-6}
6	304.3	471	0.436×10^{-7}

solid angles of the observations, because the inner lobes, middle lobe, and outer lobes are candidates for diffuse emission.

First, our flux ULs together with that of H.E.S.S. are quite low compared to the past indications of TeV gamma rays and also to the past UL measurements, demonstrating the strength of the stereo-IACT technique.

Next we discuss the total cosmic-ray energy and the cold dark matter (CDM) density for each corresponding astronomical object. Here, we assumed distances of Cen A and ω Cen to be 3.5 Mpc and 6 kpc, respectively. For the total energy of the cosmic rays, we assume that the origin of the TeV gamma-rays is the inverse Compton (IC) scattering of cosmic-ray electrons with the cosmic microwave background (CMB). The electron/proton ratio of our Galaxy is thought to be 0.1~1%. Therefore, 10^{52} erg for the electron cosmic-ray component might be a standard value for typical galaxies. Here, we assumed the electron energy spectrum of $\propto E^{-2.1}e^{-\frac{E}{E_{max}}}$. We integrate the electron spectrum greater than 1 GeV in order to calculate the total energy of electron component. The interstellar matter densities are not well measured in the corresponding regions. The electron assumption is reasonable, because the CMB density is well defined and can be considered to a lower limit for ambient photon density.

Cen A is considered to be a low-energy peaked BL Lac object (LBL) rather than high-energy peaked object (HBL). The spectral energy distribution (SED) is plotted in Fig. 4. Even if a cosmic ray flux similar to our

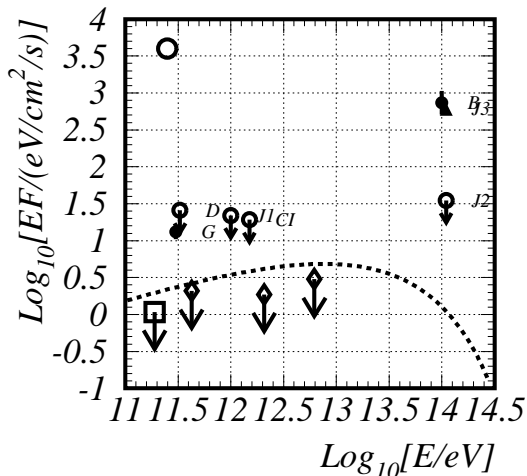


FIG. 4.— SED for the jet region of Cen A. The open circle is the prediction of Bai & Lee, (2001). The black square with the arrow is the H.E.S.S. upper limit (Aharonian et al. 2005c). The open diamonds are our upper limits. The expected gamma-ray yield with a total electron energy of 10^{54} erg with a 100 TeV cutoff energy is shown by the dashed curve. The details of the marked observations were listed in Table 1.

Galaxy's exists, there is no contradiction with any past measurements in the all wave length region (NED 2007). This, therefore, is not denying higher energy component such as 100 TeV even in the higher level compared to our Galaxy, for example 10^{53} erg of electrons. Actually, Bai & Lee, (2001) predicted a time-dependent huge energy flow in the TeV energy region which is shown by the open circle in Fig. 4. The H.E.S.S. UL is shown by the open

square with arrow and our ULs by the open diamonds. These are orders of magnitude lower than the predicted value. However, as our measurement periods correspond to a quiet phase of Cen A (from ASM data), there is no direct contradiction of this idea.

We rather concentrate ourselves to the quiet, stable, and average states of Cen A. If a high energy component of electrons $\propto E^{-2.1}e^{-\frac{E}{100\text{TeV}}}$ exists at the level of the total energy of 10^{54} erg which is one-hundred times stronger than that of our galaxy, the expected TeV gamma-ray flux is the dashed curve in Fig. 4. That is higher than our ULs, i.e. we can derive a meaningful UL to the total electron densities. The 2σ ULs (the dotted curve) for the above assumption were derived and shown in Fig. 5. The vertical scale is the logarithm of

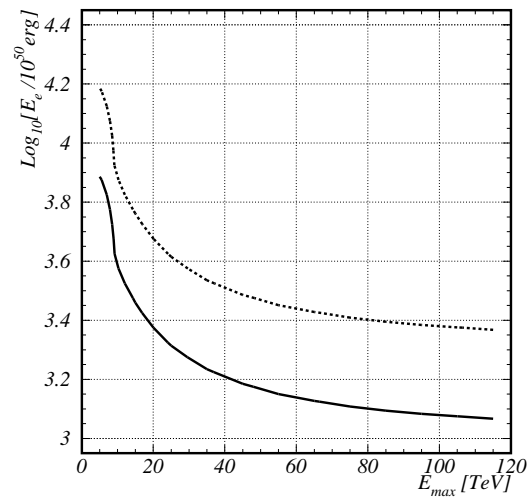


FIG. 5.— One- and two- σ upper limits to the total energy of the electron cosmic ray flux inside the jet region of Cen A versus the maximum accelerated energy. The one- σ line is the solid curve and the two- σ line is dotted.

total electronic energy normalized to 10^{50} erg and the horizontal scale is the maximum accelerated energy of the electron in TeV. At 100 TeV, the limit is 3×10^{53} erg which is thirty times bigger than that of our Galaxy. Although Cen A is highly active especially at radio, IR, and MeV energies compared to our Galaxy, any high energy cosmic-ray components are not detected; Cen A is a mysterious object. If we assume that the target photons are of those IR temperature blackbody radiation, the limits of the total energy will be significantly reduced. The future Cherenkov telescope array experiment (CTA) (CTA 2007) is promising to help resolve this, as it aims to be two orders of magnitude more sensitive than the present IACTs. If CTA does not detect any signal from this region, we might need to totally revise the idea of the cosmic-ray origin.

According to the ASM data (ASM 2007), the X-ray activity of Cen A was at a minimum in the MJD range between 53111–53113. The H.E.S.S. observation was completely coincident with this period, and ours partially. We, therefore, can divide the observational period into two, i.e., coincident with the ASM minimum, and the remaining data. The ULs for these two periods are summarized in Table 5. There is however no excess in the

TABLE 5
FLUX UPPER LIMITS IN TWO EPOCHS FOR CEN A JET

Excess Limit Events	Energy Threshold GeV	Flux Limit $\text{cm}^2 \text{s}^{-1}$	MJD-53000 day
57.6	424	0.128×10^{-10}	80, 82, 89, 91, 107
26.7	424	0.737×10^{-11}	111, 113

period of the (slightly) higher state.

ω Cen is the biggest and oldest globular cluster inside our Galaxy. There is no ionizing gas which is considered to be an origin of cosmic rays. We, therefore, do not expect any TeV radiation from this object. However, to know the minimum level of cosmic-ray density is important. There may be a lot of milli-second pulsars as has been found in other globular clusters. The object may still hold a CDM halo (Peebles 1984), as these are not clearly denied at the present level of measurements. The ULs for the total energy of electron cosmic ray component is derived in the same way as described previously. Under the assumption of a maximum electron accelerated energy of 100 TeV, the total electron energy is less than 4×10^{47} erg, i.e., less than one-supernova level, a surprisingly quiet object considering its total mass of $\sim 5 \times 10^6 M_\odot$ (van de Ven et al 2006; Meylan et al. 1995; Richer et al. 1991).

Cen A is a massive object and ω Cen a much higher density object than our Galaxy as a whole. The upper limit study of the CDM density would provide meaningful information as to the mechanism of their formations. However note that for the case of globular clusters, CDM was considered to be stripped off via tidal force in the periodic motions inside the parasite galaxy. Peebles (1984) discussed the existence of the dark matter in this kind of object. The CDM search was carried out following the procedure of Enomoto et al (2003). Here we additionally used the EGRET UL at 189 MeV (NED 2007). This is effective around the sub-TeV CDM particle mass region. Assuming the CDM particle mass of 1 TeV, the $2\text{-}\sigma$ upper limit for the CDM density is $1.2 M_\odot/\text{pc}^3$. These are quite high compared to our local density estimation of CDM of $0.01 M_\odot/\text{pc}^3$. The mass of Cen A was estimated to be several $\times 10^{11} M_\odot$ (Mathieu et al. 1996; Peng et al. 2004a,b; Karachentsev et al. 2007; Woodley 2006). In order to derive the total mass of the CDM, we multiply by a factor of $1.42 \times 10^{13} \text{ pc}^3$ considering our angular resolution of $\theta^2=0.06 \text{ degree}^2$ with an assumption of the distance of 3.5 Mpc (Hui et al. 1993). Then the total CDM mass inside the volume is less than $2 \times 10^{13} M_\odot$, i.e., a meaningless result.

For ω Cen, we can carry out the same discussion and the results are shown in Fig. 6. The result is one order of magnitude higher than that of Cen A. This is due to distance of 6 kpc compared to that of Cen A of 3.5 Mpc while the volumes are determined by the same angular resolution of the observation. However, multiplying the volume factor of $4 \times 10^4 \text{ pc}^3$, then the most CDM-particle-mass region is under its total gravitational mass of $5 \times 10^6 M_\odot$. In most regions of CDM particle mass between 100 GeV and 10 TeV, we can reject the hypothesis that the gravitational mass is dominantly occupied by the CDM particles, they might be absorbed by our

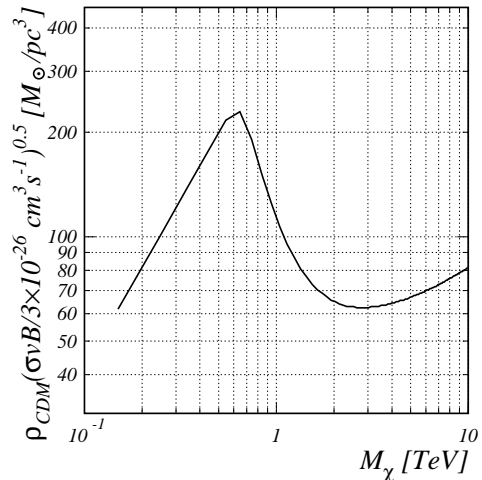


FIG. 6.— Upper limits of the CDM density versus particle mass assumption for ω Cen.

Galaxy. Presently, high energy physicists believe that the CDM particle mass lies inside the above region. The future CTA project (CTA 2007) would reveal the fact in a wider mass region, or the near-future LHC project might give a conclusive result on this subject. In cosmological life, the larger eats the smaller but its core remains.

7. CONCLUSION

In this paper, we present the results of stereoscopic observations of Centaurus A and ω Centauri with the CANGAROO-III telescopes. The observation period was 2004 March 16 to April 19 and the total observation times were 640 min for Cen A and 600 min for ω Cen. The observation of Cen A was carried out over a similar period to that of H.E.S.S. The ω Cen observations are the first reported trial by Imaging Atmospheric Cherenkov Telescopes. The analysis was carried out inside a one-degree (radius) circle from the average pointing position. We derived flux upper limits for regions containing the jet and inner lobes, the middle lobe, and portions of the outer lobes of Cen A, and center of ω Cen. The Cen A upper limits are, as with the H.E.S.S. limit, an order of magnitude lower than previous measurements.

The upper limits for the total energy of the electron components of cosmic rays were calculated under the assumption of Inverse Compton Scatterings on the cosmic microwave background, with limits of 3×10^{53} and 4×10^{47} erg obtained for Cen A and ω Cen, respectively.

Finally we gave upper limits to the density of Cold Dark Matter (CDM). Around the TeV region, we obtained upper limits of its density of $2 M_\odot \text{pc}^{-3}$ for Cen A and $100 M_\odot \text{pc}^{-3}$ for ω Cen. The limit for Cen A was greater than its gravitational mass, however, that for ω Cen was less than it.

This work was supported by a Grant-in-Aid for Scientific Research by the Japan Ministry of Education, Culture, Sports, Science and Technology, the Australian Research Council, JSPS Research Fellowships, and Inter-

University Researches Program by the Institute for Cosmic Ray Research. We thank the Defense Support Center

Woomera and BAE Systems.

REFERENCES

- Abe, K., et al. 2001, PRL, 87, 101801
 Aharonian, F. A., et al. 1999, A&A, 349, 11
 Aharonian, F. A., et al. 2005, Science, 307, 1938
 Aharonian, F. et al., 2005c, A&A, 441, 465
 Allen, W.H. et al, 1993, Astropart. Phys., 1, 269
 Allen, W.H. et al, 1993b, ApJ., 405, 554
 ROSAT All Sky Monitor (ASM), http://xte.mit.edu/ASM_lc.html
 Bai, J. M. & Lee, M. G., 2001, ApJ, 549, L173
 Burns, J. O., Feigelson, E. D., & Schreier, E. J., 1983, ApJ, 273, 128
 Carramiñana, A., et al., 1990, A&A, 228, 327
 Clay, R. W., Dawson, B. R., Meyhandan, R. 1994, Astropart. Phys., 2, 347
 Cherenkov Telescope Array (CTA), <http://www.mpi-hd.mpg.de/htm/CTA/>
 Daum, A., et al. 1997, Astropart. Phys., 8, 1
 Dufour R. J., 1979, AJ, 84, 284
 Enomoto, R., et al. 2002b, Nature, 416, 823
 Enomoto, R., et al. 2002a, Astropart. Phys., 16, 235
 Enomoto, R. et al., 2003, ApJ, 596, 216
 Enomoto, R., Tsuchiya, K., Adachi, Y., Kabuki, S., Edwards, P. G., et al. 2006, ApJ, 638, 397
 Enomoto, R., Watanabe, S., Tanimori, T., et al. 2006, ApJ, 652, 1268
 Fisher, R. A. 1936, Annals of Eugenics, 7, 179
 Graham J. A., 1979, ApJ, 232, 60
 Grindlay, J. E., Helmken, H. F., Hanbury Brown, R., Davis, J., Allen, L. R. 1975, ApJ, 197 L9.
 Hillas, A. M. Proc. 19th Int. Cosmic Ray Conf. (La Jolla) 3, 445
 Hui X., Ford H. C., Ciardullo R., and Jacobi G. H. 1993, ApJ, 414, 463
 Jones D. L. et al. 1996, ApJ. 466, L63
 Kabuki, S., et al. 2003, Nucl. Instrum. Meth., A500, 318
 Karachentsev I.D. et al., 2007, AJ, 133, 504
 Kawachi, A., et al. 2001, Astropart. Phys., 14, 261
 Mathieu A., Dejonghe H., Hui X., 1996, A&A, 309, 30
 Meylan G., Mayor M., Duquenois A., Dubath P., 1995, A&A, 303,761
 Morganti R., 1992, MNRAS, 256, 1p
 NASA/IPAC Extragalactic Database (NED), <http://nedwww.ipac.caltech.edu/>
 Peebles, P.J.E., 1984, ApJ, 186, 467
 Peng E.W. et al., 2004, ApJ, 602, 685
 Peng E.W. et al., 2004, ApJ, 602, 705
 Protheroe, R. J. 1986, MNRAS, 221, 769
 Richer H.B., Fahlman G.G., Buonanno R., Fusi Pecci F., Searle I., Thompson I.B., 1991, ApJ, 381, 147
 Rowell G. P., 1999, Astropart. Phys., 11, 217
 SkyView, <http://skyview.gsfc.nasa.gov/>
 Tanimori, T., et al. 2005, Proc. 29th Int. Cosmic Ray Conf. (Pune), OG2.2, 215
 Turner, T. J., George, I. M., Mushotzky, R. F., & Nandra, K. 1997, ApJ, 475, 118
 van de Ven G., van den Bosch R.C.E., Verolme E.K., de Zeeuw P.T., 2006, A&A, 445, 513
 Weekes, T. C., et al. 1989, ApJ, 342, 379
 Woodley K., 2006, AJ, 132, 2424